

Axionic Electroweak Baryogenesis

Kwang Sik Jeong,^{1,*} Tae Hyun Jung,^{2,†} and Chang Sub Shin^{2,‡}

¹*Department of Physics, Pusan National University, Busan 46241, Korea*

²*Center for Theoretical Physics of the Universe,
Institute for Basic Science (IBS), Daejeon, 34126, Korea*

An axion can make the electroweak phase transition strongly first-order as required for electroweak baryogenesis even if it is weakly coupled to the Higgs sector. This is essentially because the axion periodicity naturally allows the structure of phase transition to be insensitive to the axion decay constant that determines the strength of axion interactions. Furthermore, the axion can serve as a CP phase relevant to electroweak baryogenesis if one introduces an effective axion coupling to the top quark Yukawa operator. Then, for f between about TeV and order 10 TeV, the observed baryon asymmetry can be explained while avoiding current experimental constraints. It will be possible to probe the axion window for baryogenesis in future lepton colliders and beam-dump experiments.

Electroweak baryogenesis (EWBG) is one of the most attractive ways to explain the observed baryon asymmetry of the Universe [1–3]. For successful EWBG, the Standard Model (SM) needs to be extended so that the electroweak phase transition (EWPT) is strongly first-order and an extra source of CP violation is present [4–10]. The connection to EWPT has led to consider new physics near the electroweak scale with significant couplings to the Higgs sector. However, it would then be difficult to reconcile EWBG with the observed properties of the SM-like Higgs boson and LHC null results for new particle searches so far while avoiding the constraints from electric dipole moments (EDM) in association with CP violation relevant to baryogenesis.¹

In this paper we present a scenario for EWBG where an axion ϕ weakly coupled to the Higgs sector induces a required strong first-order phase transition. The potential of the extended Higgs sector possesses a discrete shift symmetry, $\phi \rightarrow \phi + 2\pi f$, and is written

$$V = V(|H|^2, \sin \theta, \cos \theta), \quad (1)$$

where H is the Higgs doublet, and $\theta = \phi/f$. Let us consider a simple model where ϕ couples to the Higgs squared operator²

$$V_0 = \lambda |H|^4 + \mu^2 |H|^2 - M^2 \cos(\theta + \alpha) |H|^2 - \Lambda^4 \cos \theta, \quad (2)$$

and so ϕ plays a crucial role in EWPT for $0 < \mu^2 < M^2$. The potential shape is determined by the constant phase α and the ratio between M and Λ , but is insensitive to f as the dependence on it arises only radiatively. This

has an important implication that the phase transition in the weak coupling limit, i.e. at large f , is not SM-like differently from other scenarios. If one increases f , the field distance between potential minima gets large at the same time, $|\Delta\phi| = f|\Delta\theta| \sim f \gg |\Delta H|$, and consequently the structure of phase transition remains approximately the same. This explains why EWBG is viable even if ϕ feebly couples to the Higgs sector.

One may wonder if a singlet scalar can play a similar role in EWPT as the axion. Let us consider a simple extension with a singlet s where the high temperature potential develops a minimum at $s = H = 0$, and a singlet-dependent Higgs mass squared is negative in a finite range of s . We assume that the Higgs mass squared has a minimum at $s = s_0$ and the electroweak vacuum appears there. A first-order phase transition is achieved if the potential has a proper profile in the region between $s = 0$ and $s = s_0$. It is possible to suppress the singlet coupling to H while maintaining the shape of the potential $V(|H|^2, s/s_0)$, if one increases s_0 accordingly and imposes a specific hierarchical relation among singlet couplings.

How large can f be without spoiling EWBG? It turns out that a strong first-order phase transition is possible for f even larger than 10^6 GeV. A more stringent bound comes from the observed baryon asymmetry. To implement EWBG, one needs sizable CP violation at the phase interface, which can be provided for instance by an effective axion coupling to the top quark Yukawa operator. In such case, the axion itself corresponds to the CP phase and should have f lower than order 10 TeV to generate sufficient baryon asymmetry during phase transition. This is because the wall width increases with f , which reduces baryon asymmetry for a given source of CP violation. On the other hand, a lower bound on f comes from the Higgs searches and results because ϕ mixes with the Higgs boson, and also from the EDM searches associated with the CP violation for baryogenesis. Those constraints can be avoided for f above about 1 TeV. For f in the multi-TeV range, it would be possible to probe our scheme by future experiments for axion-like particle

¹ The limit on electron EDM has recently been improved by about one order of magnitude [11], constraining more severely the conventional EWBG scenarios.

² The axion-dependent potential terms can be generated nonperturbatively in a controllable way, for instance, see Ref. [12]. An example of a UV completion for the effective axion couplings to the Higgs squared (2) and to the top quark Yukawa operator (8) is presented in the appendix.

searches.

For large f above the electroweak scale, H is much heavier than ϕ . Thus, for a qualitative understanding of a phase transition, one can approximately explore EWPT using the effective potential of a single light field, ϕ , constructed by integrating out the heavy Higgs field via its equation of motion, i.e. by replacing H with the classical solution of $\partial V(H, \theta)/\partial H = 0$ [13]:

$$\hat{V} = -\Lambda^4 \cos \theta + \Delta V(\theta), \quad (3)$$

which is parameterized by

$$\Lambda, \quad \alpha, \quad \epsilon \equiv \frac{\sqrt{2\lambda}\Lambda^2}{M^2}, \quad (4)$$

for μ fixed by imposing the Higgs vacuum expectation value, $v = 246$ GeV, at temperature $T = 0$. Here we take $\alpha \geq 0$ without loss of generality. To simplify our discussion, we further approximate thermal corrections to include only those to the Higgs mass squared. Then, ΔV is non-vanishing in the interval of θ where $M^2 \cos(\theta + \alpha)$ is larger than the thermal-corrected Higgs mass squared. The effective potential of ϕ is enough to discern which region of the parameter space leads to a strong first-order phase transition. After a qualitative description of EWPT, we provide precise results taking a two-field dimensional analysis with full one-loop thermal corrections.

The upper plot of Fig. 1 illustrates how a first-order phase transition is driven by the axion. At high temperature (blue curve), a large thermal mass for H leads to $\Delta V = 0$, and the minimum of \hat{V} is located at $\theta = 0$. An interval of θ where H is tachyonic appears and increases as the Universe cools down, and two degenerate minima are developed at $\theta = 0$ and θ_c at the critical temperature T_c (orange curve). The electroweak minimum, $\theta = \theta_c$, becomes the true vacuum at a temperature below T_c because it is deeper than the symmetric one, $\theta = 0$. In the lower plot, we show the contour plot of the potential at $T = T_c$ in the (θ, h) plane. The potential develops two minima separated by a barrier, and its behavior along the dashed line is described by \hat{V} .

Let us explicitly examine the parameter region where EWPT is strongly first-order for the case with $\Lambda = 130$ GeV. In the white region of Fig. 2, the axion-Higgs coupling induces a strong first-order phase transition, i.e. $v_c/T_c > 1$, where v_c is the Higgs vacuum expectation value at T_c . The blue region leads to no phase transition since the symmetric minimum is deeper than the electroweak minimum, while the green region leads to the same situation as in the SM phase transition. In the red region, a first-order phase transition takes place, but not strong. The orange region is excluded because there is a potential barrier between two minima at $T = 0$. If there remains a barrier at $T = 0$, the vacuum transition rate is significantly suppressed for f above TeV, making the

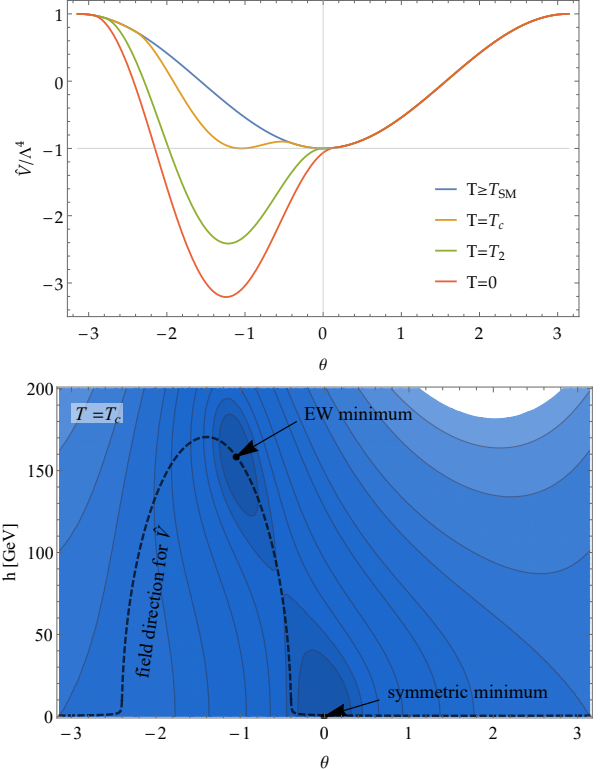


FIG. 1. Temperature-dependent potential for $\Lambda = 80$ GeV, $\alpha = 1.4$ and $\epsilon = 0.4$. Here we have approximated thermal corrections to include only those to the Higgs mass squared. In the upper plot, which shows the effective potential \hat{V} , the blue curve is for $T \geq T_{\text{SM}}$ with T_{SM} being the SM critical temperature. The yellow, green and red curve are the potentials at $T = T_c$, T_2 and 0, respectively. The lower plot is the potential at $T = T_c$ in the axion and Higgs field space, where brighter color represents a higher potential value and \hat{V} describes the potential along the dashed line.

symmetric minimum metastable. For concreteness in the later discussion of baryogenesis, we choose a benchmark parameter point

$$\Lambda = 130 \text{ GeV}, \quad \alpha = 1.4, \quad \epsilon = 0.8, \quad (5)$$

as marked by a star in the figure. The benchmark case leads to a strong phase transition, $v_c/T_c \simeq 3$, with $T_c \simeq 68$ GeV and $T_2 \simeq 54$ GeV. Here T_2 denotes the temperature at which the barrier disappears. One also finds that the axion mass reads $m_\phi \simeq 17 \text{ GeV} \times (f/\text{TeV})^{-1}$, and the axion-Higgs mixing angle is given by $\delta \simeq 0.1 \times (f/\text{TeV})^{-1}$, which makes the axion detectable at colliders. The estimated values are slightly changed depending on f if one includes radiative and other thermal contributions in the potential.

Now we move on to analyzing the phase transition in detail and examining the constraints on f . Electroweak bubbles of the broken phase are nucleated at a temperature below T_c and expand. The bubble nucleation rate

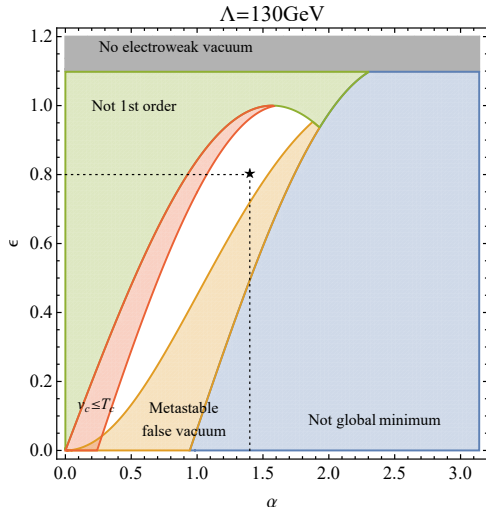


FIG. 2. EWPT for $\Lambda = 130$ GeV. A strong first-order phase transition occurs in the white region. The symmetric minimum is deeper than the electroweak minimum in the blue region, while it is metastable in the orange region. The green and red regions are excluded because the transition is not first-order as in the SM, and is weak first-order, respectively.

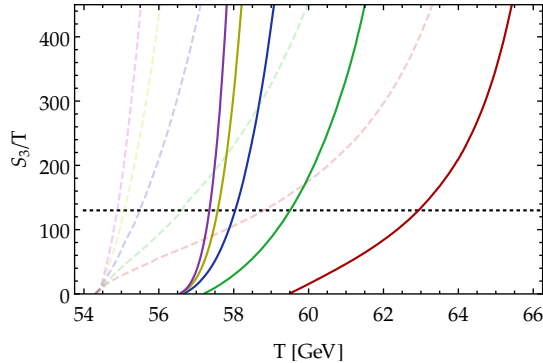


FIG. 3. Bubble action for the benchmark case (5). The solid lines show S_3/T for $f = 0.2, 0.5, 1, 1.5, 2$ TeV from right to left, respectively, where full one-loop thermal corrections have been included. The dashed lines are obtained by taking only thermal corrections to the Higgs mass squared. The dotted horizontal line is added to estimate T_n .

per unit volume is roughly given by $T^4 e^{-S_3/T}$, and it exceeds the Hubble rate when $S_3/T \approx 130$, which defines the nucleation temperature T_n . Here S_3 is the Euclidean action of an $O(3)$ -symmetric critical bubble [14, 15]. Note that $S_3 = 0$ below T_2 because there is no potential barrier between two minima.

Fig. 3 shows S_3/T as a function of T for various values of f in the benchmark case (5), where we have used the `cosmoTransition` python package to find a bubble solution through the overshooting-undershooting method [16]. The dashed lines are obtained simply by the poten-

tial $V_0(h, \phi)$ including only the thermal corrections to the Higgs mass squared, for which $T_2 \simeq 54$ GeV regardless of f as one can see in the figure. On the other hand, the solid lines show the bubble action evaluated by taking the full one-loop potential of h and ϕ at finite temperature [17], $V(h, \phi)$, which depends radiatively on f . The nucleation temperature is determined by the intersection of each solid line with the dotted horizontal line, and it approaches to T_2 as f increases. Here the barrier disappearing temperature is given by $T_2 \simeq 57$ GeV.

It is interesting to notice that the Higgs contributions to the bubble action can be approximated by integrating out the Higgs field since the importance of its kinetic term gets suppressed as f increases. Consequently, S_3 is approximately given by f^3 times some function of Λ , α , ϵ and T . This feature can be understood because the action is written

$$S_3 = 4\pi f^3 \int x^2 dx \left(\frac{h'^2}{2f^2} + \frac{\theta'^2}{2} + V(h, \theta) \right), \quad (6)$$

showing that the Higgs contribution from h' is suppressed by f^2 . Here V includes radiative and thermal corrections, and the prime denotes a derivative with respect to $x \equiv r/f$ with r being the radial distance from the center of the bubble. The approximate scaling behavior, $S_3 \propto f^3$, reflects the fact that the effective potential $\hat{V}(\phi)$ can describe well the phase transition and the tunneling occurs mainly along the axion direction if ϕ is much lighter than h , that is, for large f .

Our scenario leads to T_n rather close to T_2 compared to other scenarios, but the duration of phase transition, Δt_{PT} , is short enough to complete the first-order phase transition before the barrier disappears. In fact, a more relevant requirement is that the time scale of generating baryon asymmetry, Δt_{BG} , should satisfy

$$m_\phi^{-1} < \Delta t_{\text{BG}} < \Delta t_{\text{PT}}, \quad (7)$$

where we have used that it takes time $\sim m_\phi^{-1}$ for ϕ to settle down to the true vacuum after quantum tunneling. Since baryogenesis takes place outside bubbles via electroweak sphaleron processes, its time scale is the inverse sphaleron rate in the symmetric phase, $\Delta t_{\text{BG}} \sim T^3/(\Gamma_{\text{sph}}/V)$, where $\Gamma_{\text{sph}}/V \propto T^4$ is the sphaleron rate per unit volume [18, 19]. For large f , the bubble action shows the scaling behavior, $S_3 \propto f^3$, and S_3/T is approximately linear in T during the phase transition. It thus follows that the duration of phase transition, which corresponds to the inverse of the time derivative of S_3/T [20], is roughly given by $\Delta t_{\text{PT}} \sim 10^{-2} \times (M_{\text{Pl}}/T^2)(\text{TeV}/f)^3$, where M_{Pl} is the reduced Planck mass. Note that the above condition (7) puts an upper bound on f because both m_ϕ and Δt_{PT} are sensitive to f . For the benchmark case, baryogenesis requires f below or around 10^6 GeV.

To evaluate baryon asymmetry generated during the phase transition, one needs to specify the source of CP

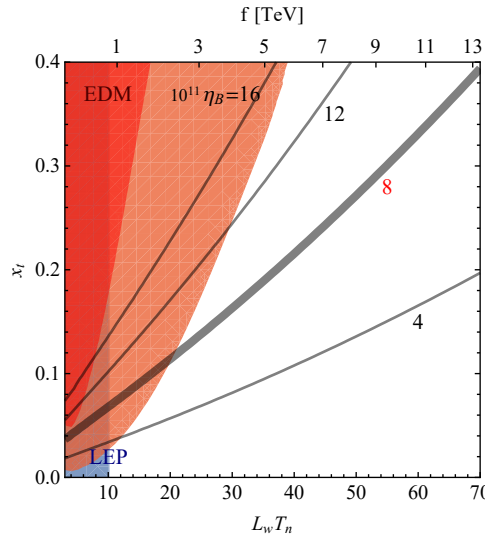


FIG. 4. Baryon asymmetry for the benchmark case (5) in the presence of an effective axion coupling to the top quark Yukawa operator. The red region is ruled out by the electron EDM constraint from ACME I [26], which requires $|d_e| < 8.7 \times 10^{-29}$ ecm, while the light red region is ruled out by the recent measurement of ACME II, $|d_e| < 1.1 \times 10^{-29}$ ecm [11]. The blue region is not compatible with the LEP results for Higgs searches.

violation. In our scenario, the axion mixes with the Higgs boson and its field value changes during phase transition. Taking this into account, we introduce an axion coupling to the top quark Yukawa operator, $e^{i\theta} \bar{q}_{L3} t_{R3} H$, to get CP violation for baryogenesis.³

The effective top quark Yukawa coupling is then written

$$Y_t = y_t + x_t e^{i(\theta+\beta)}, \quad (8)$$

for positive constants y_t and x_t , taking an appropriate field redefinition. Thus, the axion plays the role of a CP phase, and the top quark acquires a mass whose phase varies across the wall depending on the bubble profile. Note that the above axion coupling is subject to the EDM constraints if there is a relative phase between the Higgs and axion couplings to the top quark, that is, between $y_t + x_t e^{i\theta_0+\beta}$ and $i x_t e^{i\theta_0+\beta}$ with $\theta_0 = \langle \phi \rangle/f$ at $T = 0$ [24–26]. It is clear that the EDM constraints depend on β , but EWBG is insensitive to it for $x_t \ll 1$ because what matters in baryogenesis is the phase difference of the top quark mass across the wall.

For the benchmark case, we show in Fig. 4 the parameter region where the correct amount of baryon asymmetry

is obtained while avoiding the electron EDM constraint. Here we have taken $\beta \simeq -\theta_0$ so that the EDM contribution from the axion is maximized. The observed baryon asymmetry, $\eta_B = (8.2 - 9.4) \times 10^{-11}$, can be explained for f below around 10 TeV if one takes $x_t < 0.3$. One can also see that the EDM constraint is important only for f around or below TeV. If one takes a different value of β , the EDM constraint gets weaker, and the generated baryon asymmetry is slightly modified by a factor of order unity for x_t above 0.1. It should be noted that η_B is sensitive to the bubble dynamics, and our results are obtained under the assumptions summarized below. A more careful study will be necessary to estimate the relic baryon asymmetry precisely.

The analysis assumes that the bubble profiles for h and ϕ are approximated by a kink, $1 - \tanh(z/L_w)$, where z is the distance from the wall. The wall width L_w is numerically obtained by examining the S_3 critical bubble configuration, or equivalently S_4 as a time evolution of S_3 after bubble formation [14], and the relation between f and L_w is shown in Fig. 4. For a thick wall with $L_w T_n > 10$, the numerical computation suffers from instability when finding an inhomogeneous solution of the transport equations [27–31], and so we estimate the baryon asymmetry by performing an extrapolation, $\eta_B \propto x_t (L_w/L_0)^{n_1+n_2 \ln(L_w/L_0)}$, with constants n_i and L_0 .⁴ The baryon asymmetry also relies on the wall velocity v_w at a stationary situation, which can be computed based on the fluctuation-dissipation theorem using that the pressure on the wall [32] is determined by the potential difference between the broken and symmetric phases. We find that the benchmark case leads to $v_w \simeq 0.07$.

Let us continue to discuss the experimental constraints on the axion properties and the future testability of our scenario. The LHC measurements [33], which require the Higgs signal strength relative to the SM prediction to be above 0.8, constrain axion-Higgs mixing and Higgs decay into axions. For the benchmark case, one needs f above 340 GeV, and the lower bound on f would increase to 1.4 TeV if the Higgs signal rate is measured at a sub-percent level in future lepton colliders [34]. A more stringent constraint comes from the Higgs searches at LEP because axion-Higgs mixing allows the process, $e^+e^- \rightarrow Z\phi$ [35]. In the benchmark case, ϕ should be lighter than about 20 GeV to avoid the LEP bound, implying $f > 850$ GeV. For $2m_\mu < m_\phi \lesssim 5$ GeV, there is also an important constraint coming from rare meson decays, in particular from $B^+ \rightarrow K^+ \mu^+ \mu^-$. To evade it,

³ There are EWBG scenarios where the evolution of a misaligned axion field induces CP violation for baryogenesis [21–23].

⁴ In this paper we shall focus on the case where baryon asymmetry is mostly produced away from a bubble wall after diffusion. If the wall is much thicker, with $L_w T_n \gtrsim 100$, diffusion effects are less important and the dominant contribution to baryon asymmetry is generated across the wall. A successful realization of baryogenesis in such a limit has recently been discussed in Ref. [13].

one needs $\text{Br}(\phi \rightarrow \mu^+ \mu^-) \times \sin^2 \delta \lesssim 6 \times 10^{-7}$ [37], implying roughly $\sin \delta \lesssim 2 \times 10^{-3} \times (m_\phi/\text{GeV})$. The constraint is thus strong for $f > 3.4$ TeV in the benchmark case, but is avoidable if ϕ couples to the QCD anomaly or a hidden sector.

For the case that ϕ changes the phase of the top mass, there is a constraint coming from cosmology and beam-dump experiments searching for axion-like-particles if the axion has an anomalous coupling to photons, $\phi F \tilde{F}$ [36]. Those constraints rule out m_ϕ smaller than 0.5 GeV, from which we find the upper bound on f to be about 35 TeV in the benchmark case. It is thus weaker than the bound from the observed baryon asymmetry. In the presence of an axion-photon coupling, axion-Higgs mixing generates extra EDMs [37, 38]. It should be emphasized that our model naturally avoids the EDM constraints for f above about 3 TeV because the baryon asymmetry is suppressed by $1/f^n$ with $n < 1$, whereas the axion-induced EDM is strongly suppressed by $1/f^2$. As denoted in Fig. 4, although the ACME II experiment has recently improved the limit on electron EDM by one order of magnitude, our model for baryogenesis is still viable in a wide range of parameter space and does not require any accidental cancellation.

Taking into account the constraints discussed above, we find that the viable range of the axion mass is approximately between 1.3 GeV and 20 GeV in the benchmark case, which is obtained for the axion with f between 0.85 TeV and 13 TeV. Interestingly, recasting the present LHC data to the search for axion-like particles sets limits on f for the indicated axion mass range [39, 40]. High-luminosity LHC collisions are thus expected to probe our scenario. The axion window can also be tested at future lepton colliders [41].

Finally, we comment on how the viable parameter range changes when one considers a case different from the benchmark case. If one moves away from the orange region in Fig. 2, T_n and T_2 get higher, and thus the Higgs vacuum expectation value at T_n decreases and the phase transition is weakened. As a result, the size of CP violation associated with the top quark is reduced during phase transition, lowering the upper bound on f . On the other hand, if one approaches to the orange region, the upper bound on f can be released, but instead, successful baryogenesis would require tuning of the parameters. The benchmark case has been chosen to implement baryogenesis without severe tuning while allowing large f as possible. On the other hand, the lower bound on m_ϕ becomes weaker if one takes smaller ϵ since the axion-Higgs mixing is proportional to it. In this case, the LHC constraints on the Higgs properties get stronger than the LEP bound, restricting severely the parameter space to give, for instance, $m_\phi \lesssim \mathcal{O}(40)$ GeV for $\epsilon \sim 0.2$.

In this paper we have explored an axion-extended Higgs sector where EWPT is strengthened enough to implement EWBG even when the axion is feebly coupled to

the Higgs sector. This is owing to the axion periodicity, which makes the profile of the scalar potential insensitive to the strength of axion interactions. The structure of phase transition remains approximately the same under the change of the value of f . It is also interesting that the axion itself can serve as a CP phase for EWBG if one considers an effective axion coupling to the top quark Yukawa operator. In such case, axion-induced EWBG can account for the observed baryon asymmetry of the Universe while evading the current experimental constraints if f lies in the range between about TeV and order 10 TeV. Note that roughly the axion mass reads $m_\phi \sim v^2/f$, and the axion-Higgs mixing angle is given by $\sin \delta \sim \alpha v/f$. Therefore it will be possible to probe our scenario by future lepton colliders and beam-dump experiments.

Acknowledgments This work was supported by IBS under the project code, IBS-R018-D1 (THJ and CSS), and by the National Research Foundation of Korea (NRF) grant funded by the Korea government (MSIP) (NRF-2018R1C1B6006061) (KSJ). THJ and CSS thank to Eibun Senaha, Ryusuke Jinno, Fa Peng Huang and Mengchao Zhang for useful discussions.

Appendix

Let us discuss how to generate effective axion couplings relevant to axionic electroweak baryogenesis. The axion-dependent potential terms

$$-\Lambda^4 \cos \theta - M^2 \cos(\theta + \alpha) |H|^2 \quad (9)$$

have been considered to make electroweak phase transition strongly first-order, and the axion coupling to the top quark Yukawa operator

$$x_t e^{i\theta} H q_3 t^c \quad (10)$$

has been added as an example of CP violation for baryogenesis. Here we have used two-component Weyl spinors. It is obvious that the above interactions break shift symmetry, $\theta \rightarrow \theta + (\text{constant})$, but respect the discrete shift symmetry, $\theta \rightarrow \theta + 2\pi$, as required by the axion periodicity.

It is possible to generate the axion interactions in a controllable way if one considers nonperturbative effects breaking the axion shift symmetry. As an explicit example, we consider additional vector-like lepton doublets $L + L^c$ and singlets $N + N^c$ which are charged under a hidden QCD confining at Λ_c , and have interactions

$$y H L N^c + y' H^\dagger L^c N + m_L L L^c + m_N N N^c. \quad (11)$$

Note that the above interactions preserve the axion shift symmetry. For $m_N < \Lambda_c < m_L$, the heavy lepton doublets are integrated out to induce an effective mass term

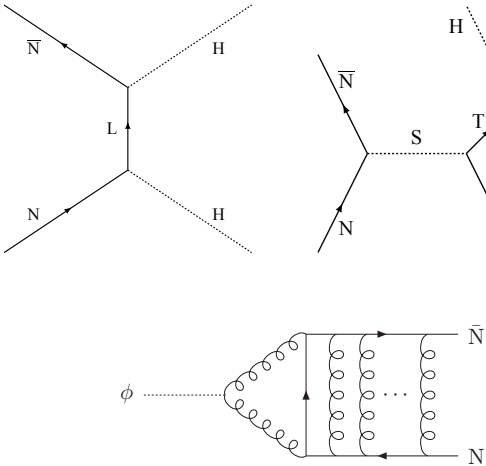


FIG. 5. Feynman diagrams for effective axion couplings. After hidden quarks $N + \bar{N}$ condensate, the axion mixes with the hidden meson (lower panel) due to the anomalous axion coupling to hidden QCD, and consequently couples to the Higgs squared operator (upper left panel) and to the top quark Yukawa operator (upper right panel).

for $N + N^c$,

$$\left(m_N + \frac{yy'}{m_L} |H|^2 \right) NN^c. \quad (12)$$

The axion shift symmetry can be anomalous under hidden QCD if it is linearly realized and spontaneously broken while making some hidden quarks massive. Then, the axion has a coupling

$$\frac{1}{32\pi^2} \theta F \tilde{F}, \quad (13)$$

where F is the field strength of hidden QCD, and \tilde{F} is its dual. The light hidden quarks $N + N^c$ condensate at Λ_c , breaking the associated chiral symmetry. As a result, there arise potential terms,

$$-\Lambda_c^4 \cos(\theta_N + \theta) - \left(m_N + \frac{yy'}{m_L} |H|^2 \right) \Lambda_c^3 \cos \theta_N, \quad (14)$$

at energy scales below Λ_c . Here $\theta_N \equiv \arg(NN^c)$ denotes the meson field. The first term induces axion-meson mixing, and thus leads to

$$\Delta V_{\text{eff}} \approx - \left(m_N + \frac{yy'}{m_L} |H|^2 \right) \Lambda_c^3 \cos \theta, \quad (15)$$

after integrating out the heavy meson. It should be noted that the effective axion coupling to the Higgs squared operator is controllable because it vanishes in the limit that the hidden QCD gauge coupling goes to zero. The Feynman diagrams for the effective axion coupling are presented in Fig. 5.

The axion coupling to the top Yukawa operator can be generated in a similar way. Let us introduce lepton

singlets $N + N^c$, vector-like top quark partners $T + T^c$, and a real scalar S with masses, m_N , m_T , and m_S , respectively. They have interactions

$$\lambda SNN^c + \lambda' STt^c + \kappa H\bar{q}_3 T^c, \quad (16)$$

which preserve the axion shift symmetry. For $m_T, m_S \gg m_N$, it is straightforward to see that the low energy effective theory of $N + N^c$, which are colored under hidden QCD, is described by

$$\left(m_N + \frac{2\kappa\lambda\lambda'}{m_S^2 m_T} H q_3 t^c \right) NN^c. \quad (17)$$

For $m_N < \Lambda_c$, the hidden quarks condensate to give

$$\Lambda_c^4 \cos(\theta_N + \theta) + \left(m_N + \frac{2\kappa\lambda\lambda'}{m_S^2 m_T} H q_3 t^c \right) \Lambda_c^3 \cos \theta_N, \quad (18)$$

where the first term arises from the axion anomalous coupling to hidden QCD. Thus, integrating out the heavy meson θ_N leads to

$$\Delta \mathcal{L}_{\text{eff}} \approx \left(m_N + \frac{2\kappa\lambda\lambda'}{m_S^2 m_T} H q_3 t^c \right) \Lambda_c^3 \cos \theta, \quad (19)$$

showing that the axion couples to the top Yukawa operator, which is essentially due to axion-meson mixing induced by the axion anomalous coupling to hidden QCD that breaks the axion shift symmetry. Fig. 5 illustrates how the effective axion coupling to the top Yukawa operator arises.

The mass parameters in the potential (9) and the coupling in the interaction (10) are given in terms of the couplings of high energy theory,

$$\begin{aligned} \Lambda^4 &= m_N \Lambda_c^3, \\ M^2 &= \frac{yy' \Lambda_c^3}{m_L}, \\ x_t &= \frac{2\kappa\lambda\lambda' \Lambda_c^3}{m_S^2 m_T}, \end{aligned} \quad (20)$$

and the constant phase α in (9) is determined by $\arg(yy') - \arg(m_N m_L)$. Hence the benchmark case with $\Lambda = 130$ GeV, $M = 100$ GeV and $x_t = \mathcal{O}(0.1)$ is obtained for instance by taking $\Lambda_c \sim \text{TeV}$, $m_N \sim 0.3$ GeV, $m_L \sim 100$ TeV, and $m_S \sim m_T \sim 2$ TeV for Yukawa couplings of order unity.

* ksjeong@pusan.ac.kr

† thjung0720@ibs.re.kr

‡ csshin@ibs.re.kr

- [1] V. A. Kuzmin, V. A. Rubakov and M. E. Shaposhnikov, Phys. Lett. **155B**, 36 (1985).
- [2] M. E. Shaposhnikov, JETP Lett. **44**, 465 (1986) [Pisma Zh. Eksp. Teor. Fiz. **44**, 364 (1986)].
- [3] M. E. Shaposhnikov, Nucl. Phys. B **287**, 757 (1987).

- [4] Y. Aoki, F. Csikor, Z. Fodor and A. Ukawa, Phys. Rev. D **60**, 013001 (1999) [hep-lat/9901021].
- [5] F. Csikor, Z. Fodor and J. Heitger, Phys. Rev. Lett. **82**, 21 (1999) [hep-ph/9809291].
- [6] M. Laine and K. Rummukainen, Nucl. Phys. Proc. Suppl. **73**, 180 (1999) [hep-lat/9809045].
- [7] M. Gurtler, E. M. Ilgenfritz and A. Schiller, Phys. Rev. D **56**, 3888 (1997) [hep-lat/9704013].
- [8] M. B. Gavela, P. Hernandez, J. Orloff and O. Pene, Mod. Phys. Lett. A **9** (1994) 795 [hep-ph/9312215].
- [9] P. Huet and E. Sather, Phys. Rev. D **51**, 379 (1995) [hep-ph/9404302].
- [10] M. B. Gavela, P. Hernandez, J. Orloff, O. Pene and C. Quimbay, Nucl. Phys. B **430**, 382 (1994) [hep-ph/9406289].
- [11] V. Andreev *et al.* [ACME Collaboration], Nature **562**, no. 7727, 355 (2018).
- [12] P. W. Graham, D. E. Kaplan and S. Rajendran, Phys. Rev. Lett. **115**, no. 22, 221801 (2015) [arXiv:1504.07551 [hep-ph]].
- [13] K. S. Jeong, T. H. Jung and C. S. Shin, arXiv:1811.03294 [hep-ph].
- [14] S. R. Coleman, Phys. Rev. D **15**, 2929 (1977) Erratum: [Phys. Rev. D **16**, 1248 (1977)].
- [15] N. Turok, Phys. Rev. Lett. **68**, 1803 (1992).
- [16] C. L. Wainwright, Comput. Phys. Commun. **183**, 2006 (2012) [arXiv:1109.4189 [hep-ph]].
- [17] M. Quiros, hep-ph/9901312.
- [18] P. B. Arnold and L. D. McLerran, Phys. Rev. D **36**, 581 (1987).
- [19] M. D'Onofrio, K. Rummukainen and A. Tranberg, Phys. Rev. Lett. **113**, no. 14, 141602 (2014) [arXiv:1404.3565 [hep-ph]].
- [20] A. Megevand and S. Ramirez, Nucl. Phys. B **919**, 74 (2017) [arXiv:1611.05853 [astro-ph.CO]].
- [21] V. A. Kuzmin, M. E. Shaposhnikov and I. I. Tkachev, Phys. Rev. D **45**, 466 (1992). doi:10.1103/PhysRevD.45.466
- [22] N. Craig and J. March-Russell, arXiv:1007.0019 [hep-ph].
- [23] G. Servant, Phys. Rev. Lett. **113**, no. 17, 171803 (2014) doi:10.1103/PhysRevLett.113.171803 [arXiv:1407.0030 [hep-ph]].
- [24] J. Brod, U. Haisch and J. Zupan, JHEP **1311**, 180 (2013) [arXiv:1310.1385 [hep-ph]].
- [25] K. Fuyuto, J. Hisano and E. Senaha, Phys. Lett. B **755**, 491 (2016) [arXiv:1510.04485 [hep-ph]].
- [26] J. Baron *et al.* [ACME Collaboration], Science **343**, 269 (2014) [arXiv:1310.7534 [physics.atom-ph]].
- [27] M. Joyce, T. Prokopec and N. Turok, Phys. Rev. Lett. **75**, 1695 (1995) Erratum: [Phys. Rev. Lett. **75**, 3375 (1995)] [hep-ph/9408339].
- [28] J. M. Cline, M. Joyce and K. Kainulainen, JHEP **0007**, 018 (2000) [hep-ph/0006119].
- [29] D. Bodeker, L. Fromme, S. J. Huber and M. Seniuch, JHEP **0502**, 026 (2005) [hep-ph/0412366].
- [30] L. Fromme and S. J. Huber, JHEP **0703**, 049 (2007) [hep-ph/0604159].
- [31] S. Bruggisser, T. Konstandin and G. Servant, JCAP **1711**, no. 11, 034 (2017) [arXiv:1706.08534 [hep-ph]].
- [32] P. B. Arnold, Phys. Rev. D **48**, 1539 (1993) [hep-ph/9302258].
- [33] G. Aad *et al.* [ATLAS Collaboration], Eur. Phys. J. C **76**, no. 1, 6 (2016) [arXiv:1507.04548 [hep-ex]].
- [34] H. Baer *et al.*, arXiv:1306.6352 [hep-ph].
- [35] T. Flacke, C. Fruguele, E. Fuchs, R. S. Gupta and G. Perez, JHEP **1706**, 050 (2017) [arXiv:1610.02025 [hep-ph]].
- [36] S. Alekhin *et al.*, Rept. Prog. Phys. **79**, no. 12, 124201 (2016) [arXiv:1504.04855 [hep-ph]].
- [37] K. Choi and S. H. Im, JHEP **1612**, 093 (2016) [arXiv:1610.00680 [hep-ph]].
- [38] M. Jung and A. Pich, JHEP **1404**, 076 (2014) [arXiv:1308.6283 [hep-ph]].
- [39] S. Knapen, T. Lin, H. K. Lou and T. Melia, arXiv:1709.07110 [hep-ph].
- [40] A. Mariotti, D. Redigolo, F. Sala and K. Tobioka, Phys. Lett. B **783**, 13 (2018) [arXiv:1710.01743 [hep-ph]].
- [41] J. Jaeckel and M. Spannowsky, Phys. Lett. B **753**, 482 (2016) [arXiv:1509.00476 [hep-ph]].